CP1195, *Shock Compression of Condensed Matter - 2009*,
edited by M. L. Elert, W. T. Buttler, M. D. Furnish, W. W. Anderson, and W. G. Proud

SHOCK TEMPERATURES OF PREHEATED MgO

Oleg V. Fat'yanov[1], Paul D. Asimow[2], and Thomas J. Ahrens[1]

[1]*Lindhurst Laboratory of Experimental Geophysics, Seismological Laboratory, MC 252-21,*
[2]*Division of Geological and Planetary Sciences, MC 170-25,*
California Institute of Technology, Pasadena CA 91125

Abstract. Shock temperature measurements via optical pyrometry are being conducted on <100> single-crystal MgO preheated before compression to 1905-1924 K. Planar shocks were generated by impacting hot Mo(driver plate)-MgO targets with Mo or Ta flyers launched by the Caltech two-stage light-gas gun up to 6.6 km/s. Quasi-brightness temperature was measured with 2-3% uncertainty by a 6-channel optical pyrometer with 3 ns time resolution, over 500-900 nm spectral range. A high-power, coiled irradiance standard lamp was adopted for spectral radiance calibration accurate to 5%. In our experiments, shock pressure in MgO ranged from 102 to 203 GPa and the corresponding temperature varied from 3.78 to 6.53 kK. For the same particle velocity, preheated MgO Hugoniot has about 3% lower shock velocity than the room temperature Hugoniot. Although model shock temperatures calculated for the solid phase exceeded our measurements by ~5 times the uncertainty, there was no clear evidence of MgO melting, up to the highest compression achieved.

Keywords: MgO, inductive heating, plate impact, fast optical pyrometry, equation of state, melting.
PACS: 07.20.Ka, 62.50.Ef, 64.70.dj, 91.60.Fe

INTRODUCTION

Despite its obvious importance in geophysics, the melting curve of MgO at high pressures remains essentially unknown. Only two groups have reported temperature data for this material at high pressures: shock temperature measurements in solid MgO along the principal Hugoniot from 174 to 203 GPa [1] and direct measurements of the MgO melting curve using laser-heated diamond anvil cell technique up to 31.5 GPa [2].

Numerous calculations show significantly steeper melting curves than that measured [3-5]. Predicted melting temperatures at the pressure of Earth's core-mantle boundary, 135 GPa, range from about 5000 to 8500 K [2-5]. The main goal of the current research is to get additional experimental data on the pressure dependence of MgO melting and to resolve the inconsistency.

EXPERIMENTAL PROCEDURE

This work used two previously developed methods: shock wave experiments on samples preheated up to 1923 K [6] and conventional shock pyrometry [7,8]. The layout is shown schematically in Fig. 1. The target consists of a single crystal of >99.95% pure MgO 1 cm square by about 3.1 mm thick (MTI Corp.), optically polished on two <100> faces, held tight in a cylindrical geometry, two-piece threaded assembly made of >99.97% pure Mo (H. C. Starck Inc., ABL-1.75 rod specifications). The first part forms a 1 mm thick driver plate and 14.3 mm inner diameter sample chamber. The second part is a 22 mm outer diameter cap with a beveled opening, 4 mm in diameter, at the center for outgoing light intensity measurements. Good mechanical contact, MgO sample integrity, and heating uniformity were checked in about 10 separate heat tests. Pinhole-

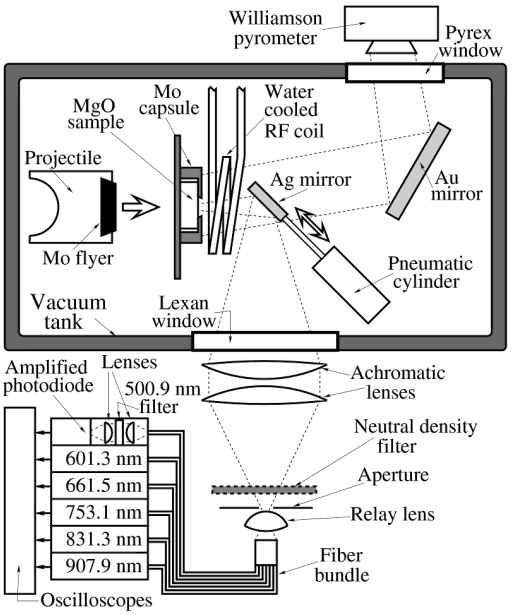

Figure 1. Experimental schematic in firing configuration. Flat, 3-turn pancake-shaped heating coil is drawn out-of-plane and is shown displaced from target for clarity.

free Ti foil (Alfa Aesar), about 13 μm thick, sealed the gap between hot Mo and MgO.

The 6-channel pyrometer is of imaging/non-imaging type with double spatial optical averaging [9,10]. Two 50 cm focal length, *f*/4.7 achromatic doublets form an 0.8x demagnified target image on the surface of a 20 mm focal length, *f*/1 biconvex relay lens. The latter images the almost uniformly bright area of the second achromat on the fiber bundle face. This makes the first stage of optical averaging via a classic slide projector scheme. A thin, 2 mm diameter aperture close to the relay lens selects the pyrometer field of view.

The second stage of spatial averaging is implemented by a randomized, 6-branch custom multiple fiber bundle (Oriel Corp.). Every branch goes to an individual light-tight, imaging wavelength selection unit affixed to its amplified photodetector (New Focus, model 1801, 3 ns rise time, DC-125 MHz bandwidth at 3 dB). Each unit has two identical collimating and focusing plano-convex glass lenses (15 mm focal length, *f*/1.3) and a 10 nm FWHM bandpass filter. Electronic signals are recorded on Tektronix DPO 4034 oscilloscopes (350 MHz analog bandwidth, 2.5 GHz sampling rate). The detector-amplifier response to input light power is linear to 1.5 V; a typical noise level is under 30 mV peak-to-peak.

For absolute intensity calibration of the pyrometer (not shown in Fig. 1) we used a 900 W coiled-coil irradiance standard lamp (Optronic Laboratories, Inc., model S-1045) as a secondary radiance standard [10]. We cross-calibrated a 0.5x demagnified image of this spatially non-uniform lamp against a N.I.S.T.-traceable source of spectral radiance (Optronic Laboratories, Inc., model 550G) using our pyrometer and a 6½ digit Keithley 2000 multimeter. Validity of the whole calibration procedure, accurate to ±5% absolute intensity, was checked in a test shot on <100> NaCl (see Table 1). Our temperature datum agrees to 1% with the values from Ref. 11.

The final part of the experimental cycle was similar to that in [6]. The target was gradually heated by a manually-controlled 10 kW induction heater over 15-20 minutes. The sample was held at the desired temperature for about 5 minutes to reach thermal equilibrium. Target temperature, measured over the 18 mm diameter central area of the Mo cap, was continuously monitored until a

TABLE 1. Summary of our experimental parameters and main results.

Shot	Flyer	U_f, m/s	Driver	T_0, K	Target	U_s, km/s	U_p, km/s	P, GPa	T, kK	dT/dr, kK
383[a)]	Mo	6540±7	Mo	1905±3	MgO	11.9±0.2	4.390±0.015	174±5	5.7±0.3	1.6
384[a)]	Mo	6081±5	Mo	1924±3	MgO	11.59±0.11	4.085±0.010	158±4	5.2±0.3	1.4
386	Cu	6434±3	Cu	294±2	NaCl	10.00±0.05	4.694±0.007	102±1	7.25±0.17	2.4[b)]
387	Mo	4563±6	Mo	1924±3	MgO	10.31±0.14	3.099±0.010	106±3	3.75±0.10	0.7
389	Mo	5093±4	Mo	1914±3	MgO	10.80±0.11	3.441±0.010	124±3	4.37±0.08	1.0
390	Mo	4401±8	Mo	1914±3	MgO	10.26±0.10	2.986±0.010	102±2	3.78±0.07	0.7
391	Ta	6589±11	Mo	1912±3	MgO	12.72±0.13	4.798±0.011	203±4	6.53±0.13	1.9

[a)]Irradiance calibration type of measurements [7,8], 4 pyrometer channels at 500.9, 601.3, 753.1, and 907.9 nm.
[b)]Measured value of r=0.03±0.01 from Ref. 15 was used in Eq. 1.

few seconds before the shot by a dual-wavelength Williamson pyrometer (model 8120S-C-T, 710 and 810 nm, 1 K resolution).

DATA ANALYSIS

The shock states in the samples were calculated from measured projectile velocities, known Hugoniots for cold and hot Mo [6], and measured shock velocities in hot MgO. Hugoniots for cold Ta and Cu, used in some experiments, were taken from [12]. Dimensions and densities of hot Mo and MgO were recalculated from initial values using reported thermal expansion data [13,14] and measured target temperatures.

The true spectral radiance data from shot 389 are shown in Fig. 2. A shock wave enters the MgO at 0 ns and reaches the free surface at 290 ns. An optically thick radiative layer [15] is established in 20-30 ns, depending on the wavelength. After that, until about 220 ns, all radiance histories remain essentially constant. This indicates better than ±10 K initial temperature uniformity in MgO for at least 2 mm thickness. A gradual temperature decrease by 60 K at 220-290 ns, common to all channels, is also seen in shot 390 (Fig. 3) but not in shots 383 and 384. It is caused by initially lower temperature in the bigger aperture area in later experiments. The effect of this cold-spot introduces negligible errors in measured shock velocities and does not influence our temperature measurements that used the steady radiance values before 220 ns.

Shock temperatures were extracted for each channel [15,16] by solving the equation

$$I(\lambda)=(1-R)(1-r)/(1-R\cdot r)\cdot N(T,\lambda), \quad (1)$$

where $I(\lambda)$ is the measured spectral radiance, $N(T,\lambda)$ is the Planck black-body spectral radiance, T is the shock temperature, λ is the wavelength, R is the Fresnel reflectivity of MgO-vacuum interface, and r is the shock front reflectivity. Negligible spectral dependence of MgO refractive index at our conditions allowed us to use the same average value of R=0.076 for all channels. High temperature refractive index data were taken from [17,18]. Since no shock front reflectivity data are available yet, for analysis we consider the highest value of r = 0.02 predicted by Gladstone-Dale relationship [15]. For different r, possible corrections to our lower limit, quasi-brightness temperatures can be calculated using dT/dr values listed in Table 1. Comparison of temperatures extracted from different channels was one of the cross-checks for our measurements. A good agreement between the values (see Figs. 2,3) confirmed that the necessary condition for thermal equilibrium was satisfied [15,16].

RESULTS AND DISCUSSION

Parameters from 7 shots are listed in Table 1. Because of large uncertainty of simple linear fit parameters, we constructed the highest U_s hot Hugoniot allowed by our data. It is shown in Fig. 4 along with the principal Hugoniot from [19]. The hot MgO Hugoniot and a Grüneisen parameter extracted from the offset between the cold and hot Hugoniots were further used to calculate shock temperatures for the conditions of our experiments and ones listed in [1]. All T vs. P results along with the reported melting data are shown in Fig. 5.

Neither U_s vs. U_p nor T vs. P data for hot MgO

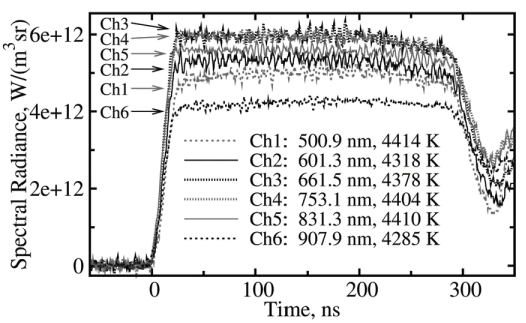

Figure 2. Spectral radiance histories from shot 389.

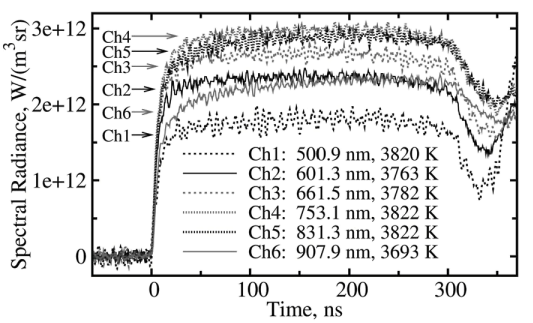

Figure 3. Spectral radiance histories from shot 390.

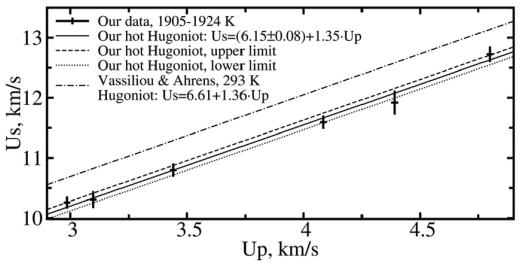

Figure 4. MgO Hugoniot summary.

revealed any discontinuity or change in slope typical of melting [8,11,15]. Calculated temperatures are 350-1000 K higher than the measured values at equal pressure; the discrepancy increases at higher shock pressure (Fig. 5). About 50% more light from shocked MgO is required to make a match. For the Grüneisen values we used (γ=1.5 at $3\cdot10^{-4}$ m^3/kg specific volume and constant γ/V), predicted temperatures along the principal MgO Hugoniot are also somewhat higher than reported in Ref. 1.

CONCLUSIONS

We demonstrate the first ±1.0-1.5% Hugoniot shock velocity and ±2-3% quasi-brightness shock temperatures for single crystal MgO preheated to 1905-1924 K. To achieve this, we had to develop several techniques first. Accurate absolute intensity pyrometer calibration by a non-uniformly bright light source, highly uniform sample preheat, and suppression of light flash from shock wave closure of the hot Mo-MgO interface are only some of them to mention. The obvious discrepancy between

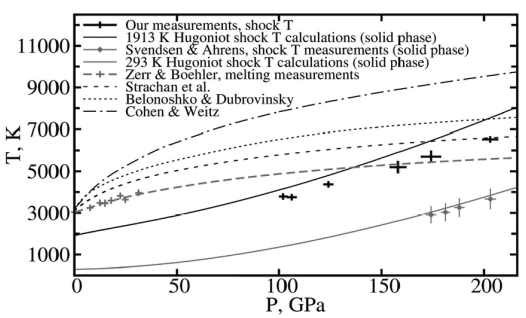

Figure 5. Summary of MgO shock temperature data and reported melting curves.

our measured and predicted temperatures may be caused by shock front reflectivity or improper Grüneisen function. Available data show no clear evidence of melting, up to the highest 203 GPa and $6.53\cdot10^3$ K achieved.

ACKNOWLEDGEMENTS

We thank M. Long, E. Gelle, and R. Oliver for valuable technical assistance. Funding was provided by the U.S. NSF, grant EAR-0810116.

REFERENCES

1. Svendsen, B. and Ahrens, T. J., *Geophys. J. R. astr. Soc.* **91**, 667-691 (1987).
2. Zerr, A. and Boehler, R., *Nature* **371**, 506, (1994).
3. Strachan, A., Çağin, T., and Goddard III, W. A., *Phys. Rev. B* **60**, 15084-15093 (1999).
4. Belonoshko, A. B. and Dubrovinsky, L. S., *Am. Mineral.* **81**, 303-316 (1996).
5. Cohen, R. E. and Weitz, J. S., *Geophysical Monograph* **101**, 185-196 (1998).
6. Asimow, P. D., Sun, D., and Ahrens, T. J., *Phys. Earth Planet. Inter.* **174**, 302-308 (2009).
7. Gupta, S. C., Love, S. G., and Ahrens, T. J., *Earth Planet. Sci. Lett.* **201**, 1-12 (2002).
8. Luo S.-N. et al., *J. Geophys. Res.* **109**, B05205, doi:10.1029/2003JB002860 (2004).
9. DeWitt, D. P. and Nutter, G. D., *Theory and Practice of Radiation Thermometry* (Wiley, New York, 1988), pp. 242-252, 262-268.
10. Holmes, N. C., *Rev. Sci. Instrum.* **66**, 2615-2618 (1995) and reference 7 therein.
11. Lyzenga, G. A., Ph. D. thesis, California Institute of Technology (1980).
12. Mitchell, A. C. and Nellis, W. J., *J. Appl. Phys.* **52**, 3363-3374 (1981).
13. Reiter, P. and Kaschnitz, E., *Int. J. Thermophys.* **23**, 1327-1338 (2002).
14. Dubrovinsky, L. S. and Saxena, S. K., *Phys. Chem. Minerals* **24**, 547-550, (1997).
15. Kormer, S. B., *Sov. Phys. - Uspekhi* **11**, 229 (1968).
16. Fat'yanov, O. V. et al., *Infrared Phys. Technol.* **42**, 55-60 (2001) and references therein.
17. Zouboulis, E. S. and Grimsditch, M., *J. Geophys. Res.* **96** (B3), 4167-4170 (1991).
18. Saenger, K. L. and Gupta, J., *Appl. Opt.* **30**, 1221-1226 (1991).
19. Vassiliou, M. S. and Ahrens, T. J., *Geophys. Res. Lett.* **8**, 729-732 (1981).